Compound events of wet and dry extremes: identification, variations, and risky patterns

Haiyan Chen[1], Ye Tuo[1], Chong-Yu Xu[2], Markus Disse[1]

1 Hydrology and River Basin Management, Technical University of Munich, Munich, Germany

2 Department of Geosciences, University of Oslo, Oslo, Norway

Abstract

Compound hydrometeorological extremes have been widely examined under climate change, they have significant impacts on ecological and societal well-being. This study sheds light on a new category compound of contrasting extremes, namely compounding wet and dry extremes (CWDEs). The CWDEs are characterized as devastating dry events (EDs) accompanied by wet extremes (EWs) in a given time window. Notably, we first adopt a separate system to identify coinciding events considering the different evolving processes and impacting patterns of EDs and EWs. The peak-over-threshold and standardized index methods are used in a daily and monthly window to identify EWs and EDs respectively. Furthermore, the spatial-temporal changes and risky patterns of CWDEs are fully understood by using the Mann-Kendall test, the Ordinary Least Squares, and the Global and Local Moran indices. Germany is the study case. As one major finding, the results indicate a pronounced seasonal effect and spatial clustering pattern of CWDEs. The summer is the most vulnerable period for CWDEs, and the spatial hotspots are mainly located in the southern tip of Germany, as well as in the vicinity of the capital city Berlin. Besides, robust uptrends of CWDEs in all aspects have been discovered over long periods, and the moist climate and complex geography collectively contribute to severe CWDEs. Unexpectedly, the study finds that compounding events in dry regions are mainly driven by wet extremes while they are more dependent on dry anomalies in wet regions. The research contributes to the discoveries of compound extremes which are composed of individual hazards with distinct features. Related findings will aid decision-makers in producing effective risk mitigation plans that prioritize vulnerable regions with limited resources during climate change. Lastly, the robust framework and open access data allow for extensive exploration of various compounding hazards in different regions.

Keywords

Hydrometeorological extremes, Compound hazards, Spatiotemporal variations, Risky patterns, Temperate regions,

1 Introduction

Hydrometeorological extremes (HMEs) can be characterized by significant water surplus and deficit phenomena, resulting from meteorological anomalies (Abbate et al. 2021, Ciccarese et al. 2020, Zuzani et al. 2019). Typically, dry and wet extremes, such as floods and droughts, will lead to water stress on crops and cause human beings and livestock to suffer physiological pressure (Iizumi and Ramankutty 2015, Lucas et al. 2014), and end up with ecological disturbance, agricultural losses, and socioeconomic disruption (Apurv et al. 2017, Kreibich et al. 2022, Tabari et al. 2021). In addition to the incidence of these single hazards, recent studies have been devoted to changing patterns of compound HMEs (CHMEs), such events can be interpreted as extreme impacts that depend on multiple variables or events (Leonard et al. 2013, Zhang et al. 2021, Zscheischler et al. 2018) and can produce hazardous and higher consequences than individuals types (Schumacher et al. 2019, Yang et al. 2022). Given the global hydrological cycle is expected to intensify in a warming world, possible threats will come with complex interactions of multiple extremes with upgrading intensity and magnitude (Chen et al. 2020, Gu et al. 2022, Zscheischler et al. 2019). Hence, a better understanding of CHMEs is urgently needed, particularly about their physical characteristics and potential changes, to manage relevant disasters and advance climate adaptation strategies.

Global studies have examined correlations between a variety of hazards and identified the hotspots of up to 20 kinds of CHMEs (Ridder et al. 2020, 2022). On a regional scale, many scholars have dedicated to the interplay of certain compound events, such as the attention on compound extreme dry events (EDs) (Feng et al. 2021, Mukherjee and Mishra 2021, Vogel et al. 2021, Wu et al. 2022) and compound wet extremes (EWs) (Bermudez et al. 2021, Jang and Chang 2022, Lai et al. 2021, Saharia et al. 2021). Yet, there is a real dearth of information regarding the compound events of contrasting types of HMEs, such as the CWDEs where devastating dry events are accompanied by wet extremes within a given time window (Liu et al. 2018, Shi et al. 2022). Although EDs and EWs act like incompatible hazards, they develop in the same hydrological cycle and are strongly connected to physical and societal processes across space and time (Ji et al. 2017, Tian et al. 2014). Several historical CWDEs have been documented, examples include phenomenal extremes occurring in England and Wales (Parry et al. 2013), Tasmania and Queensland in Australia (CSIRO 2014, News 2019), Yangtze River basin in China (Shan et al. 2018), etc. It is reported that such hazards often lead to more drastic ecological and socioeconomic effects (Sadegh et al. 2018, Shi et al. 2020, Visser-Quinn et al. 2019, Bi et al. 2022), including deteriorated soil water holding capacity and soil erosion (Chen et al. 2020), land degradation (Handwerger et al. 2019), water pollution (Huang et al. 2019), crop yield reduction (Bi et al. 2022), etc. Given the limited disaster management resources, scientific studies associated with CWDEs are expected to help integrate EWs' risk reduction with EDs' prevention, contributing to a more efficient and resilient socio-hydrological system.

The credible characterization of CHMEs is essential for accurate risk analysis, it requires in-depth research to enhance both theoretical frameworks and practical tools. Typically, CWDEs can be detected based on single EWs and EDs where precipitation is considered as the key factor, as it plays a key role and can be explained as the climatology of the precursors to HMEs (Anderson et al. 2019, Garg and Mishra 2019, Hellwig et al. 2020). Various standardized index methods (SIM) are used universally to identify CWDEs. For example, Shi et al. (2020) explored the combination dynamics of EWs and EDs by using the seasonal Standardized Precipitation Index (SPI); at a smaller scale, the monthly Standardized Precipitation Evaporation Index (SPEI) and self-calibrated Palmer Drought Severity Index (PDSI) were adopted to discuss the sequential or concurrent EWs and EDs (Chen et al. 2020, De Luca et al. 2020, Qiao et al. 2022). However, most research on CHMEs took the same approach with a unified time window to extract EWs and EDs simultaneously. The fact is that the two hazards have distinct evolving dynamics and impact mechanisms. Instead of the creeping and accumulative effects of EDs (Bachmair et al. 2016), a rapid process of destructive disasters could be facilitated by EWs, such as landslides and flash floods caused by days or even hours of heavy precipitation (Lin et al. 2020, Matanó et al. 2022). Adopting a longer window, even a monthly scale, may dilute the time effect of EWs and underestimate the extremity of EWs and attendant impacts. However, identifying EDs based on a shorter time window could overestimate EDs and produce a cluttered result with noise (Ho et al. 2021; Li et al. 2020). The dilemma necessitates an enhanced identification of CWDEs which can consider critical and distinct traits of EWs and EDs all at once.

To narrow the aforementioned gaps, the study focuses on the novel category of compound extremes and aims to develop a reliable identification method. Based on this, the spatiotemporal changes and driving forces of the events will be further investigated. To this end, we extract CWDEs based on the SIM and peak-over-threshold (POT) in a separate identifying window. The monthly extraction of EDs but daily detection of EWs are determined concerning the distinct evolving process and time effect between the two extremes. Furthermore, long-term investigations of EDs, EWs, and CWDEs are conducted spanning seven decades. We evaluate the temporal changes of extremes by using the Ordinary Least Squares and the Mann-Kendall test methods, and the Global and Local Moran Index is applied to explore spatial clustering patterns. Instead of studying specific CHMEs, the derived systematic overviews can assist in comprehending and detecting changes over the past (Nyeko-Ogiramoi et al. 2013) and support the sustainable management of disaster risk (Abbate et al. 2021).

Germany is selected as a case study. As a temperate region, it has received less attention compared with traditional arid and humid regions. However, the area has been witnessing more threatening HMEs due to climate change and anthropocentric influence, consequently causing serious injuries, fatalities, and economic losses (Erfurt et al. 2019, Kaiser et al. 2021, Wieland and Martinis 2020). Therefore, the research carried out will greatly benefit the study domain around prevention and early warning of CHMEs. More importantly, it will broaden insights into HMEs and provides a new angle to identify coinciding events of multiple hazards with distinct characteristics.

The rest of the paper is organized as follows. Section 2 introduces the study area and used data. In Section 3, we display the methods involving the identification of extreme events, temporal trends analysis, and spatial clustering. The results on spatiotemporal characteristics of EDs, EWs, and CWDEs are depicted in Section 4. In Section 5, we discuss further the identification, behaviors, and driving forces of CWDEs. Section 6 summarizes the primary contribution and key findings of the current work.

2 Study Area and Data

2.1 Study area

As a classic temperate region, Germany is located in the central part of Europe, spanning from 47°N to 55°N and from 5°E to15°E, as shown in Figure 1. With an area of 357,022 km^2, the study domain stretches 853 kilometers from its northern border with Denmark to the Alps in the south. Being one of the four largest food producers in the European Union (Klöckner 2020), half of the German territory is utilized for farming purposes, which makes it more vulnerable to HMEs because of potential huge crop losses. Furthermore, the elevation of the area increases from north to south (Figure 1), the highest latitude refers to 2938m. A moderately continental climate dominates the area with an increasing gradient from west to east. Both climatic and geographical conditions lead to clear patterns of precipitation, temperature, and snow coverage in the region (Merz et al. 2018).

As a temperate region, Germany experiences mean annual temperatures and precipitation averaging 10°C and 729 mm, respectively, over a long period (https://climateknowledgeportal.worldbank.org/). However, record-breaking droughts have occurred extensively in recent years, such as the events spanning 2015, 2018, 2019, and 2022 (Ihinegbu et al. 2022, Report, 2022, Schuldt et al. 2020). On the other hand, it has been observed that the development of EWs favors specific atmospheric conditions in the temperate region, manifesting as occurrences like flash floods and extreme precipitation (Meyer et al. 2020). Hence, a thorough investigation into the characteristics of HMEs becomes imperative. Such an in-depth study holds the potential to alleviate and avoid adverse effects on both the ecological environment and socio-economy.

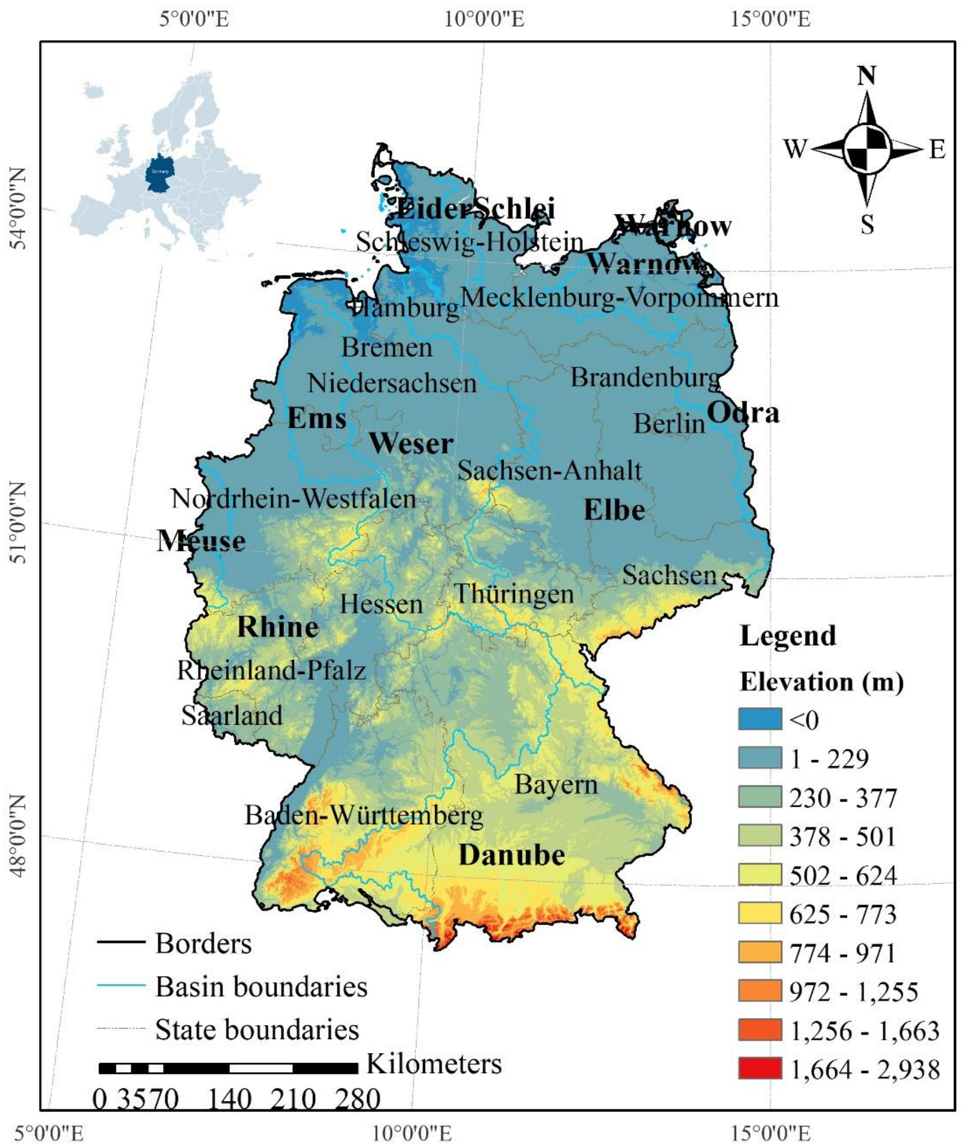

Figure 1. Overview of the study area. The national territory is divided into 16 distinct states and encompasses a complex river network of ten basins. The lowland region of northern Germany extends from the north to the foreland of the central German uplands, while the southernmost part of the country is rugged mountainous terrain.

2.2 Data

The data used in the study are from three aspects, and more information and pre-processing are described as follows.

(1) For meteorological data, long-term grided precipitation series on various space-time scales can be accessed from the ERA5-Land reanalysis datasets in the European Centre for Medium-range Weather

Forecasts (https://cds.climate.copernicus.eu/cdsapp#!/home). The study extracted daily and monthly precipitation with 0.1° spacing in both longitude and latitude for the 1950–2021 time period. Precipitation provided on the reanalyzed platform is a three - dimensional data set generated from a large number of atmospheric, land, and oceanic climate variables, which have good accuracy across Europe (Hu and Franzke 2020, Rivoire et al. 2021). In addition, the database offers a subset of other water and energy variables at equal or finer spatial resolution, such as temperate, radiation, and soil water, thereby making further continuous studies possible.

(2) The administration boundaries and divisions were obtained from BKG (2015, 2017) and LfU (2017), and the elevation data were taken from the European Environment Agency (2016).

(3) The catchment information was from the Environment Center of the European Commission (https://ec.europa.eu/environment/water/participation/map_mc/countries/germany_en.htm) where multiple dividing levels for entire European basins can be found. We integrated the details from both level 5 and level 6 to develop an authoritative distribution of the basin map, which is coordinated with the Report from the Commission to the European Parliament and the Council.

3 Methodology

To investigate CWDEs, the study first identifies the different climatic regimes from the whole area, and the extraction of the extreme events is applied to the sensitive regions selected. Based on the dataset of all extremes, the spatial distribution and temporal changes are further analyzed in detail. We classify the methodologies implemented into four main procedures, which are further elaborated in the sub-sections following.

3.1 Pooling regional climatic regimes

The dissimilar spatial features and changes in HMEs are found between dry and wet regimes (Allan et al. 2010, Donat et al. 2016). For capturing the refined differences between extremes' behaviors, the study pre-extracts wet (WRs) and dry regions (DRs) from the whole area at first. Examinating hydrometeorological variables facilitates the assessment of the long-term effects of climate change and further classification of climatic regimes (Ahmed et al. 2019, Pour et al. 2020). There are extensive methods to partition dry and wet regimes spatially (Ullah et al. 2022). One effective approach of them is based on representative values of long-series precipitation data. For example, average precipitation (Han et al. 2019, Li et al. 2023) and equivalent percentiles (33.3th and 66.67th) of precipitation series (Schurer et al. 2020) were utilized in previous studies. Here, we try to achieve a more precise and reliable partitioning result by analyzing various percentiles. With 5% as the step, the study scrutinizes all relevant percentiles of monthly precipitation over the long climatological period.

Based on precipitation distributions, we further utilize the Getis-Ord (Gi*) to delineate DRs and WRs from all grid cells. The method tests the spatial associations of the higher and lower values based on the hypothesis that spatial features are distributed randomly in the whole area (Chowdhuri et al. 2022, Qiang 2019). The statistic index, called Gi_Bin, will be returned from the calculation and can determine whether the original assumption is accepted or refused. Specifically, the statistic values corresponding to the P-value and Z-score are used to display significant confidence about the assessment for the value given. The signs of the value represent higher and lower values out of the whole area. In our application, the positive Gi_Bin values are the wet regions with higher precipitation in the long run, and vice versa for dry regions represented by the negative values. The pixels are considered reliably dry/wet regions only when they meet the entry confidence level: P≤0.5, |Gi_Bin|≥ 2. The Gi_Bin statistic is given as:

$$G_i^* = \frac{\sum_{j=1}^{n} \omega_{i,j} x_j - \bar{X} \ \sum_{j=1}^{n} \omega_{ij}}{S\sqrt{\frac{\left[n \sum_{j=1}^{n} \omega_{i,j}{}^2 - \left(\sum_{j=1}^{n} \omega_{i,j}\right)^2\right]}{n-1}}} \tag{1}$$

Where,

$$\bar{X} = \frac{\sum_{j=1}^{n} x_j}{n} \tag{2}$$

$$S = \sqrt{\frac{\sum_{j=1}^{n} x_j{}^2}{n} - (\bar{x})^2} \tag{3}$$

Gi_Bin (G_i^*) falls into [-3,3], and when $|\text{Gi\_Bin}| \geq 2$ indicates there is an over 95% statistical confidence to consider the spatial value given as a dryspot or wetspot. Lastly, we discuss all results derived from different percentiles and compare them with annual average precipitation to determine the final thresholds for classification.

3.2 Identifying extreme events

As a bivariate hazard, the CWDEs discussed are driven by EDs and EWs. The extraction procedures of EDs and EWs are separated considering the different developing procedures and influencing mechanisms. Specifically, we adopt a daily scale to pool EWs but a monthly window to detect EDs, and the identification of CWDEs is based on the concurrent scenarios of individual events. It is noted that concurrent events are not constrained to occur at the same minute strictly; they are defined as a concurrence within a limited time window. More details and reasons for identifying scales and processes are given in the following.

(1) Wet extremes

The POT is applied to find EWs on a daily scale. Since the study focuses exclusively on extreme wet anomalies, we adopt the 99^{th} percentile as the threshold that stems from the daily precipitation dataset across the nation. This choice aligns with the recommendations of the Expert Team on Climate Change Detection and Indices (ETCCDI), which advocates the 99th threshold as an index to identify extremely wet days. Compared with other commonly used thresholds, such as 90% and 95% (Kalisa et al. 2021, Xu et al. 2021. Garg and Mishra et al. 2019), the threshold is expected to provide a more precise analysis of the upper extreme parts of the precipitation series. Moreover, it is important to ensure a sufficiently high number of EWs and associated CWDEs for robust statistical analysis (Poschlod et al. 2020, Zscheischler and Seneviratne et al. 2017). Higher percentiles beyond 99% are not further considered. By limiting the threshold to 99%, the study pursues a reasonable balance between adequately representing extreme events and avoiding a scarcity of event samples. Furthermore, the extraction of EWs prescribes a minimum time lag of 10 days between two events to ensure the independence of each event (Brunner et al. 2021).

(2) Dry extremes

SPI is adopted for extracting EDs; it is a globally used index and has been recommended as a key drought indicator by the World Meteorological Organization (Wilhite 2006). The index converts the precipitation distribution to the standard normal distribution based on the equivalent accumulative probability of a given value (McKee et al. 1993). The value of SPI is interpreted as the number of standard deviations from the long-term mean, it provides an intuitive way to compare the dry severity of periods across different regions. Besides, various calculating scales of SPI, from 1 to 36 months, show great flexibility in evaluating different types of dry events (Ali et al. 2019).

The monthly detection is executed for EDs based on multiple considerations. First, the identifying scale can avoid a jumbled dataset and overestimation of EWs caused by an identification based on a shorter time window. Second, monthly identification guarantees CWDEs of sufficient quantity and quality as it is not too long to match daily-scale EWs. Lastly, the identification will not ignore the extremity of EDs, since it is an accountable window to find flash droughts indicating relatively short-term dryness but devastating phenomena (Salvador et al. 2020, Tyagi et al. 2022). Furthermore, the threshold value of EDs is set to -1.3, it is ranked as the D2 level (severe dry condition) according to the National Drought Monitor Center (North American Drought Monitor, 2018), and it is considered extreme enough for a temperate region. A lower value denotes a drier condition, which represents that the specific month deviates from the mean value of the same months in the long series by at least 1.3 standard deviations.

(3) CWDEs

The occurrence of CWDEs is characterized as a binary variable when exceptional EWs are found during the period of synchronous EDs, which is quantified as an extremely dry condition on a monthly scale accompanied by heavy rainfall lasting one to ten days. The severity of CWDEs is computed by normalized characteristics both of EWs and EDs, including number (*NUM*), magnitude (*MAG*), and intensity (*INT*). Specifically, we transform SPI values to their reciprocals due to lower values with higher intensity. All values are rescaled to the interval (0,1) in WRs and DRs, and a compound extreme index is calculated by the sum of the normalized values of the EWs and EDs. The *NUM*, *MAG*, and *INT* are calculated by the following equations:

$$NUM = \frac{TN}{TY} \tag{4}$$

$$MAG = \frac{\sum_{i=1}^{i=TN} x_i}{TY} \tag{5}$$

$$INT = \frac{NUM}{MAG} \tag{6}$$

Where *TN* represents the total number of events, *TY* means the total year, x_i is the corresponding value of the *i* th event. We mention that a lumped study is performed for CWDEs by taking whole WRs and DRs as units, since a very limited number of CWDEs is found in each grid. As a compromise, a distributed analysis is conducted for all grid cells regarding individual extremes, an accurate and comprehensive analysis of EWs and EDs is expected to help us understand the behaviors and changes of compound events.

3.3 Investigating temporal trends

The Ordinary Least Squares (OLS) method is adopted to analyze linear trends. It is a common technique for building linear models between one or more quantitative variables (Franzke 2021, Pal et al. 2011). The model quality is controlled by the F-test and the T-test, and the significance level is set as 5%. Meanwhile, the Manner-Kendall test (Kendall 1948, Mann 1945) and the Theil-Sen Median method (Sen 1968) are used to detect non-linear tendencies. Once trends are determined by the Manner-Kendall test (MK test), the Theil-Sen Median method can correspondingly produce Sen's slope to measure the rate of changes in variables' time series. The final slope is the median of all slopes obtained from all data pairs and can be calculated by following formulas (Thomas and Prasannakumar 2016):

$$T_i = \frac{x_j - x_k}{j - k} \quad (i = 1, \dots N) \tag{7}$$

$$Q = \begin{cases} T_{\frac{N+1}{2}} \\ \dfrac{\left(T_{\frac{N}{2}} + T_{\frac{N+2}{2}}\right)}{2} \end{cases} \tag{8}$$

In the equation, x_j and x_k are the values at times *j* and *k* (*j* > *k*), and *N* represents the number of pairs of time series elements. *Q* is the median of all values of slopes. A positive value *Q* indicates an increasing trend, whereas a negative represents a decreasing trend. More calculating processes regarding the MK test are included in the Supplementary and Appendix Data. As effective tools, the combination of the MK test and Sen's slope can assess if there is a monotonic positive or negative trend of the hydrometeorological variables over time (Gocic and Trajkovic 2013, Wang et al. 2020). The test process is fully non-parametric in that the data assessed do not conform to any distributions.

Additionally, the sub-interval trend assessment is conducted when no statistically significant trends exist for the whole period. Specifically, the study designs a sliding window: the starting point is the beginning of the year 1950 and the initial length of the time window is fixed to 10 years; the repetitive testing process is performed by extending the window length year by year, the round will not be ceased to enter the next round until a significant trend is detected. For example, the first significant trend is located in the interval [1950, I] (I is 1960 or larger), then a repeating process begins from the interval of [I, I+J] (J is from 10) to find the next interval depending on the appearance of significant trends. If no trend exists, the work will be terminated when the terminus (the sum of I and J) is over 2021. This frame is repeated with a dynamic starting point from 1950 to 2011.

3.4 Analyzing spatial clusters

To explore the spatial clustering patterns of CWDEs, the Global Moran's Index (GMI) and Anselin Local Moran Index (LMI) are used. The global and local autocorrelation will be discovered regarding the variables between a certain spatial region and neighboring regions (Agarwal et al. 2022, Liu et al. 2022, Treppiedi et al. 2021). Before the clustering processes, we define a new index, the comprehensive severity index (CSI), to measure the overall performance of CWDEs. Considering the equal importance of all three dimensions of events, a linear model is constructed based on equal weights of NUM, MAG, and INT.

GMI measures global auto-correlation based on both the feature locations and feature values. The index derived summarizes the overall clustering information. A positive index will be found when the dataset tends to cluster spatially, which means high values cluster near other high values and low values cluster near other low values spatially. Otherwise, there is a dispersed pattern or no random distribution for given variables. From -1 to +1, the -1 represents the perfect negative spatial autocorrelation, such as a regular pattern or dispersion, whereas the +1 describes a perfect clustering distribution (CSI in our case). The statistical reliability of the results is estimated by the z-score and p-value as well, and the significant level is determined as 5%.

Beyond the general clustering pattern provided by GMI, more directive and inner information is needed to detect which regions are similar to or different from their neighborhood. By doing that, highly risky clusters will be discovered with higher severity of CWDEs in the study area. In this case, LMI is capable of exploring significant inner clusters (significance level of 5%) among each grid cell, which could produce five categories (Table 1) including the none-significant group, high-to-high cluster (HH), low-to-low cluster (LL), high-to-low outlier (HL), and low-to-high outlier (LH).

In summary, the clustering analysis begins with the calculation of GMI to determine if an overall clustering pattern exists for the whole space of WRs and DRs. If so, inner cluster information will be further given by computing LMI. The results will specify the geographical locations of CWDEs at a high resolution, such as county-level administrations, thereby optimizing resource allocation for those vulnerable areas.

Table 1 Different implications of clusters in the Anselin Local Moran's Index

Clusters	Implications
No-significant	No significant clustering effect statistically
High-high	A high value of CSI near other neighbors with high values as well
High-low	A high value of CSI near other neighbors with low values
Low-high	A low value of CSI near other neighbors with low values
Low-low	A low value of CSI near other neighbors with low values as well

4 Results

4.1 Dry and wet regions

The 10^{th} and 90^{th} percentiles are finally determined as thresholds to denote overall conditions of dryness and wetness for each grid over the period investigated. The corresponding distribution maps are displayed in Figure B.1 in the Supplementary and Appendix Data. As relatively higher/lower thresholds in long-term series, the two values can be used to capture the abnormal wet and dry conditions (Tan et al. 2023). Meanwhile, the classification of climatic regimes produced by the combination of the two thresholds (Figure 2) is well validated by the annual average precipitation distribution in the Hydrological Atlas of Germany (Figure B.4 (b) in Supplementary and Appendix Data). The atlas, developed based on ground observations, is publicly published by the Federal Institute of Hydrology (Bundesanstalt für Gewässerkunde, https://geoportal.bafg.de).

As shown in Figure 2, out of 7142 cells (another 1039 grid pixels lack the data), 30% of Germany is identified as the more vulnerable WRs and DRs, with 70% of them being DRs. Only 9% of the national land is dominated by wetter regimes. Wet cells are mainly concentrated in the southern parts of Germany, and a few are found in the central parts of the Rhine and eastern regions in the Danube basin. In particular, more than half of the wet spots are found in the Danube basin, as validated by evidence from historical records of destructive EWs there (Becker and Grünewald 2003, Blöschl et al. 2013, Blöschl et al. 2016). On the contrary, DRs are more discretely distributed in almost all basins with various proportions (Table A.1 in the Supplementary and Appendix Data). Notably, a bulk of DRs are found in the northeastern lowlands and some southwestern regions of Germany. These areas have been characterized as vulnerable dry regions due to the significant impact caused by phenomenal EDs (Scharnweber et al. 2011, Erfurt et al. 2019, Süßel and Brüggemann, 2021, Ihinegbu and Ogunwumi, 2022).

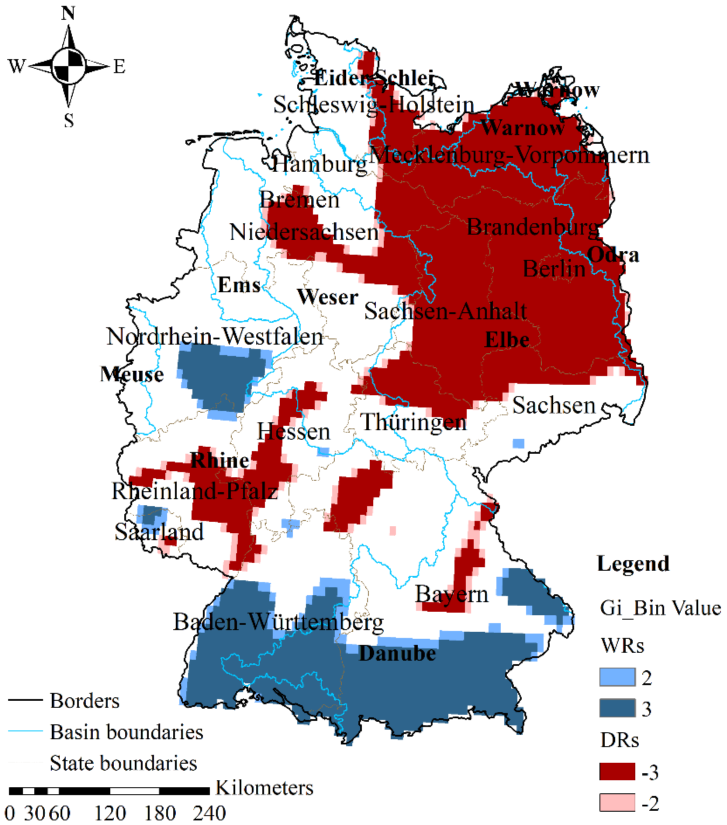

Figure 2. Agents of different climate regimes. The wetter regions are labeled by values 2 and 3, indicating a significant level of 5% and 1%. Conversely, regions are marked with -2, and -3 representing drier areas, highlighting a similar level of significance.

4.2 Individual extremes

Spatial variations of individual extremes are shown in Figure 3, including spatial distributions of the number, magnitude, and intensity of EWs and EDs. Figure 4 represents all significant trends found in WRs and DRs. As a supplement, the overall number of grids with a significant trend and the specific locations with the greatest slopes are provided in Table A.2 and Table A.3 in the Supplementary and Appendix Data, respectively. The thorough discussions of EDs and EWs will lay a solid foundation for comprehending the behaviors of CWDEs.

4.2.1 Spatial distribution

In general, the distribution patterns of the number and magnitude of EDs demonstrate spatial homogeneity. Specifically, these two variables exhibit comparable levels across different regions. In both DRs and WRs, the median of ED's number is around 1.2 (per year), and the magnitude of these events is nearly equal to -2.2 of SPI (per event). These findings are illustrated in Figures B.3 (a) and (b) in the Supplementary and Appendix Data. Nevertheless, a few higher values of EDs' number and magnitude are observed within DRs, primarily concentrated in the central Elbe basin and central-western Rhine basin (Figure 3 (a) and (b)). Furthermore, distinct clusters of EDs with high risk implications become apparent when examining the distribution of ED's intensity. The vulnerable regions, characterized by higher EDs' intensity, are situated in the Rhine basin at the west end and eastern tips of the Elbe and Odra basin in Germany. Simultaneously, some regions marked by severe EDs are also identifiable in the southwest corners of the Rhine in WRs.

Conversely, a great heterogeneity is detected in the distribution of EWs' number and magnitude. The striking gap points to the yearly magnitude where the WRs triple the events in DRs (Figures B.3 (c) and (d) in the Supplementary and Appendix Data). The southern tips of the Danube and Rhine basin in WRs are the most susceptible areas which almost hold the highest number, magnitude, and intensity of EWs. As to DRs, some regions in the Weser and Rhine basins present a scattered distribution of higher numbers and magnitude of EWs. Plus, the western parts of the Elbe basin and most of the Schlei basin in Germany from the DRs show a greater intensity of EWs.

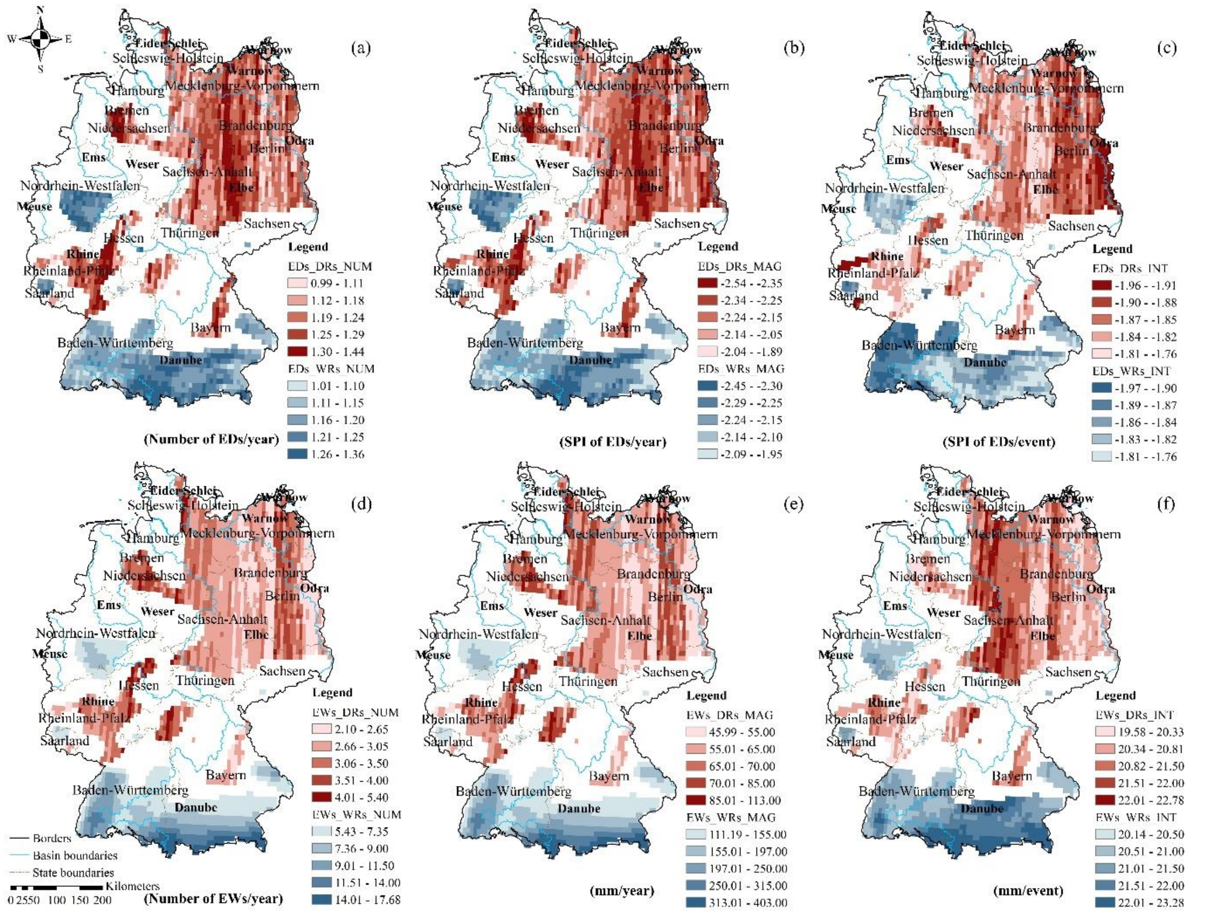

Figure 3. Spatial distributions of extreme events. Figures (a)-(c) and Figures (d)-(f) are the distributions of extreme dry (EDs) and wet events (EWs) in both dry (DRs) and wet regions (WRs), respectively. From left to right, the figures display the spatial representation of the number (NUM), magnitude (MAG), and intensity (INT) of the extreme events. For each figure, the titles adhere to a consistent naming convention, utilizing corresponding abbreviations. For example, "EDs (EWs)_DRs (WRs)_NUM" refers to the number of EDs (EWs) in DRs (WRs). In the figures, the color red is used to depict the distribution of extreme events in DRs, and blue represents WRs. Additionally, a darker shade indicates a higher level of NUM, MAG, or INT.

4.2.2 Temporal trends

(1) Extreme wet events

In general, there is an increasing trend in all significant trends of EWs, regardless of the number, magnitude, or intensity, as illustrated in Figure 4. The most prominent trends are observed when measuring EWs by magnitude, subsequently followed by slower increases in the number and intensity of EWs. In detail, the median slope values of EWs' magnitude are 0.70 and 0.45 in WRs and DRs, respectively. WRs with substantial uptrends are located in the eastern parts of Bavaria, the southeast corners of the state Nordrhein Rhine-Westphalia, and the southern state of Baden-Württemberg State in the Rhine basin. For DRs, bigger median slopes are located in the central part of Bavaria in the Danube basin and the northern part of Bavaria in the Rhine basin. Although the uptrends are evident both in magnitude and number of EWs, the average intensity of EWs remains steady both in WRs (0.03) and DRs (0.06). The generally larger uptrends suggest a larger scale of EWs in WRs, however, the study also finds some DRs have unexpectedly faster wetting steps than WRs, indicated by a more significant increasing ratio of the intensity of EWs in DRs than WRs (Figure 4 (c) and (f)).

(2) Extreme dry events

Compared to EWs, there is no drastic change in EDs, all regions remain at a steady level generally, especially for most DRs. However, subtle fluctuations are observed in some WRs, where the number of EDs shows a downward trend but the magnitude of EDs demonstrates an upward trend. About 7% of WRs show an apparent decrease in the EDs' number with slopes ranging from 0.01 to 0.02. They are distributed widely in eastern parts of Bavaria and a few are scattered in the Baden-Württemberg. Conversely, around 5% of areas of WRs witness greater uptrends in the magnitude of EDs. These pieces of evidence indicate that fewer higher-magnitude EDs have happened over the past seven decades. In DRs, the intensity of EDs sees a clear clustering pattern where 6% of DRs showing downtrends gather in the adjacent parts of the Elbe basin and Oder basin in the northern part of Brandenburg State. More visible slopes are found in the magnitude and intensity of EDs in the DRs and are located in the southeastern state of Hessen and eastern Brandenburg State, although they account for only 1% of DRs.

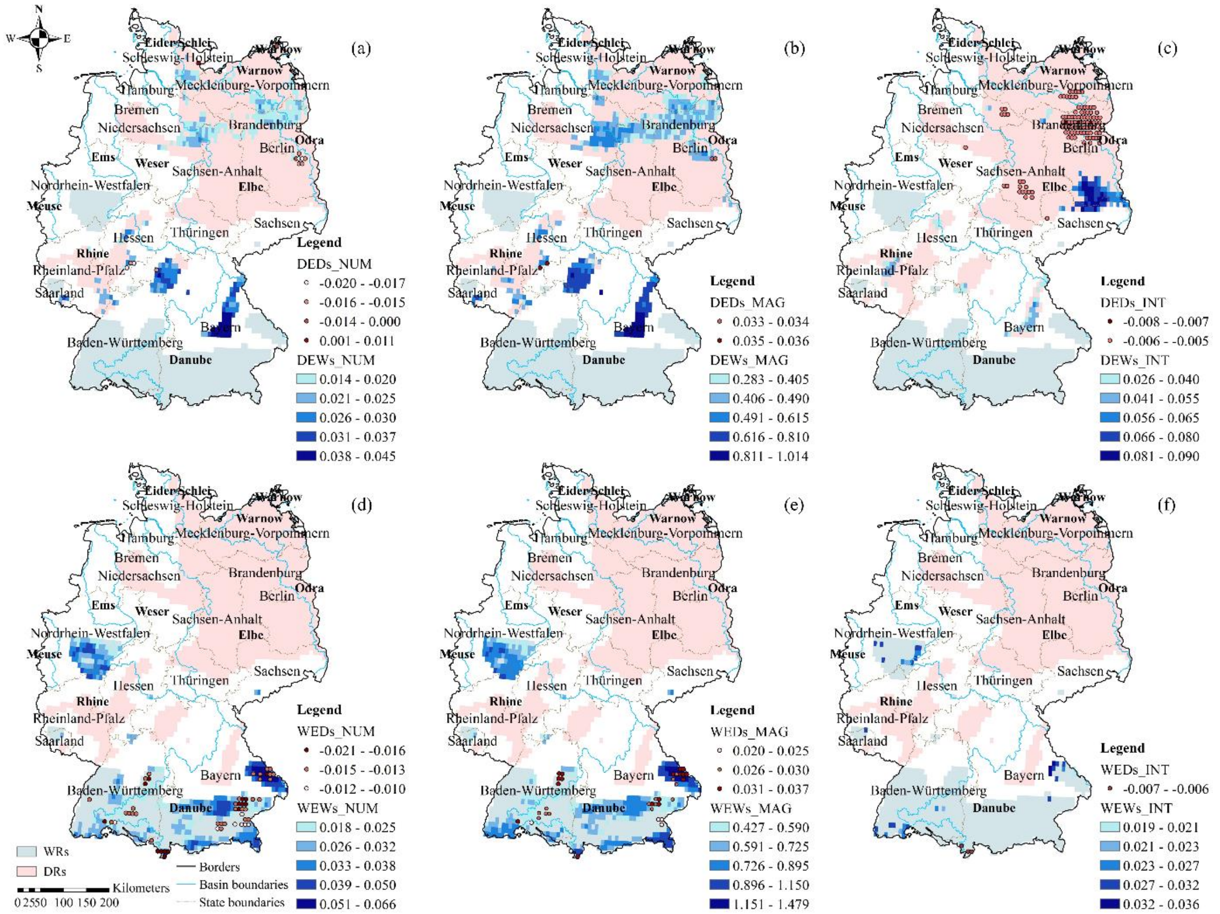

Figure 4. Significant trends of extreme events (p≤0.05). Subfigures (a)-(c) show trends of EDs and EWs in D (dry regions), and subplots (d)-(f) present the yearly changes of extreme events in W (wet areas). The column from left to right represents the temporal tendencies regarding NUM (number), MAG (magnitude), and INT (intensity) of extreme events. The units of figures are: (a) and (d): number of events/year, (b) and (e): magnitude of events/year (EDs: SPI/year, EWs: mm/year), (c) and (f): intensity of events/year (EDs: (SPI/event)/year, EWs: (mm/event)/year). The points on the red spectrum show the trends of EDs (extreme dry events) and the blue squares display the information on EWs (extreme wet events). The titles of each figure follow a consistent naming rule, utilizing corresponding abbreviations. For example, "DEDs_NUM" denotes the slopes of EDs in the number in D.

4.3 Compound extremes

4.3.1 Seasonal characteristic

The lumped analysis focuses on the seasonal behaviors of CWDEs, the result is shown in Figure 5. In total 11689 events are detected across WRs and DRs, and 80% of them are from WRs. In principle, the CWDEs' levels in WRs are far higher than the extremes in DRs, no matter in terms of number, magnitude, or intensity. The biggest difference is detected in the magnitude of CWDEs where the events in WRs exceed 14 times that of DRs, and even the smallest gap triples DRs shown in the intensity of CWDEs. Seasonal performance differentiates WRs and DRs most in autumn, and slighter differences are observed in other seasons with a declining ratio from the winter to the spring and summer.

On the other hand, the intra-year analysis indicates that around 70% of events with a higher magnitude and intensity occur in the summer. Overall, the extreme degree of CWDEs behave similarly in spring and autumn, but both of them are stronger than events found in the winter. Such rules are well confirmed by the events found in WRs. However, the events in the spring measured by all indices are more dramatic than extremes detected in the autumn when we look at DRs solely. On the monthly scale, a great consistent distribution between DRs and WRs is observed, which shows that the more severe compounds concentrate in the months from May to September, especially in June and July. However, it is noted that CWDEs could happen in all remaining months at a lower intensity.

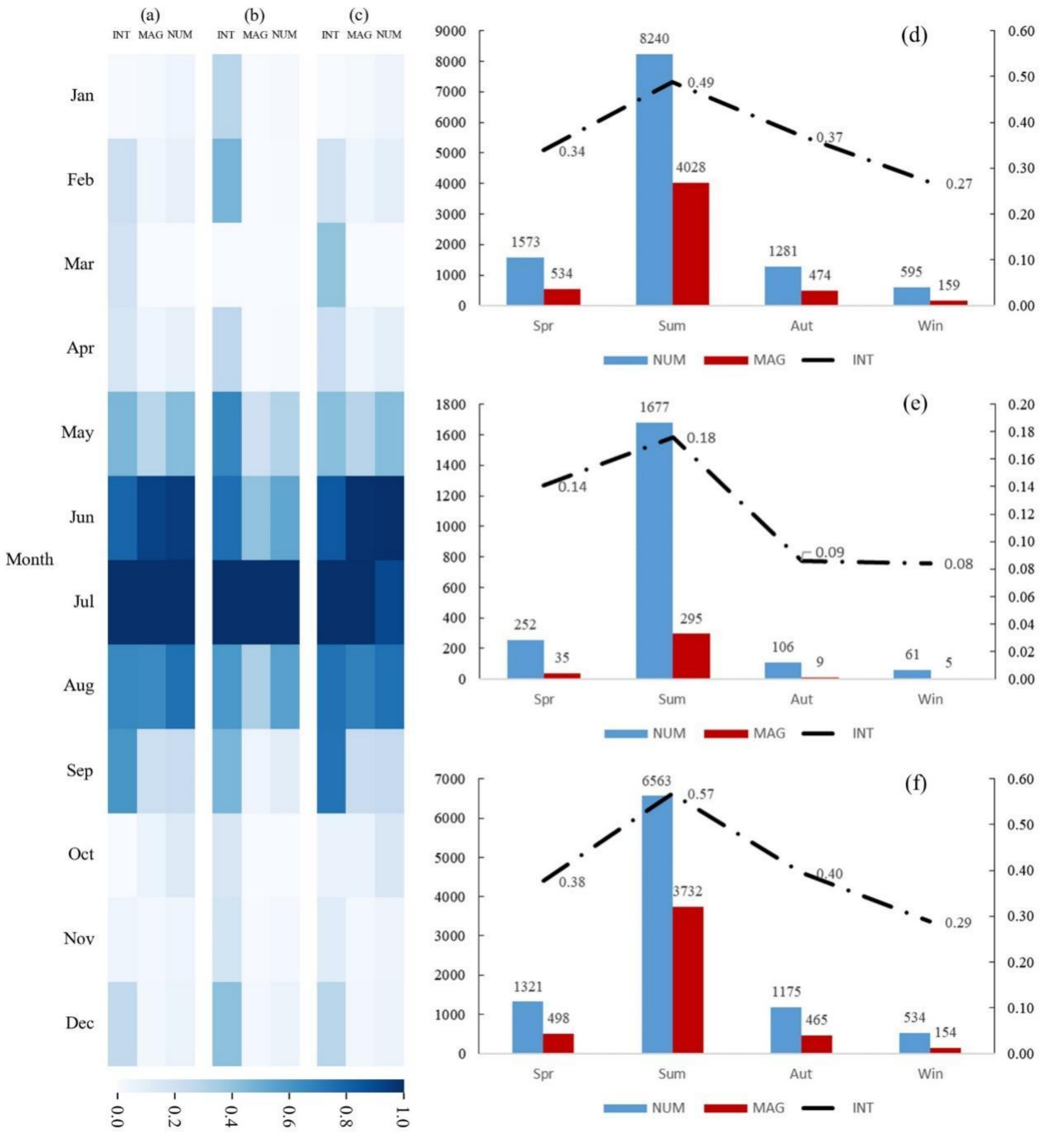

Figure 5. Intra-year changes of compounding wet and dry extremes (CWDEs) on monthly and seasonal scales. (1) Figures (a)-(c) show monthly variations of the comprehensive severity index (CSI) of events in number (NUM), magnitude (MAG), and intensity (INT). From the left to the right, the sub-plot shows features of events found in both wet and dry regions, single dry regions, and single wet regions sequentially. The shade of blue depends on the values, with a darker one showing a larger value. (2) Figures (d)-(f) represent seasonal distributions of CWDEs. From top to bottom, the sub-plot presents features of whole regions, dry regions, and wet regions respectively, and the accumulative number (NUM) and magnitude (MAG) of extremes are shown by blue and red bars, and measured by the left axis; and the black dashed line describes the average intensity (INT) changes throughout the four seasons.

4.3.2 Temporal trends

Within inter-year changes, temporal trends of yearly CWDEs are analyzed in two different climatic regimes, the results are shown in Figure 6 and Table 2. Uptrends of CWDEs are dominant both in WRs and DRs over the past seven decades. For DRs, an increasing trend of CWDEs in magnitude and intensity is confirmed by the M-K test analysis, especially a greater slope regarding the magnitude of CWDEs. There is no persistent and robust tendency in the number of CWDEs. However, two sub-intervals are located since the strikingly increasing trends are examined, as indicated by the considerable increments with a slope value of 3 from 1950 to 1973 and a slope value of 4 from 1978 to 1988.

In contrast to DRs, the number of CWDEs exhibits a continued uptrend spanning from 1953 to 2021, with a steep slope of 1.448. Alongside this notable rise in CWDEs frequency, there is a substantial increase observed in the magnitude of CWDEs during the same period, characterized by a lower growth rate compared to the number of CWDEs. Notably, the intensity of CWDEs in WRs witnesses a complex pattern of fluctuation. A pronounced increase occurs from 1962 to 1974, followed by a marked decline over the subsequent decade. However, such alternations do not recur in recent years.

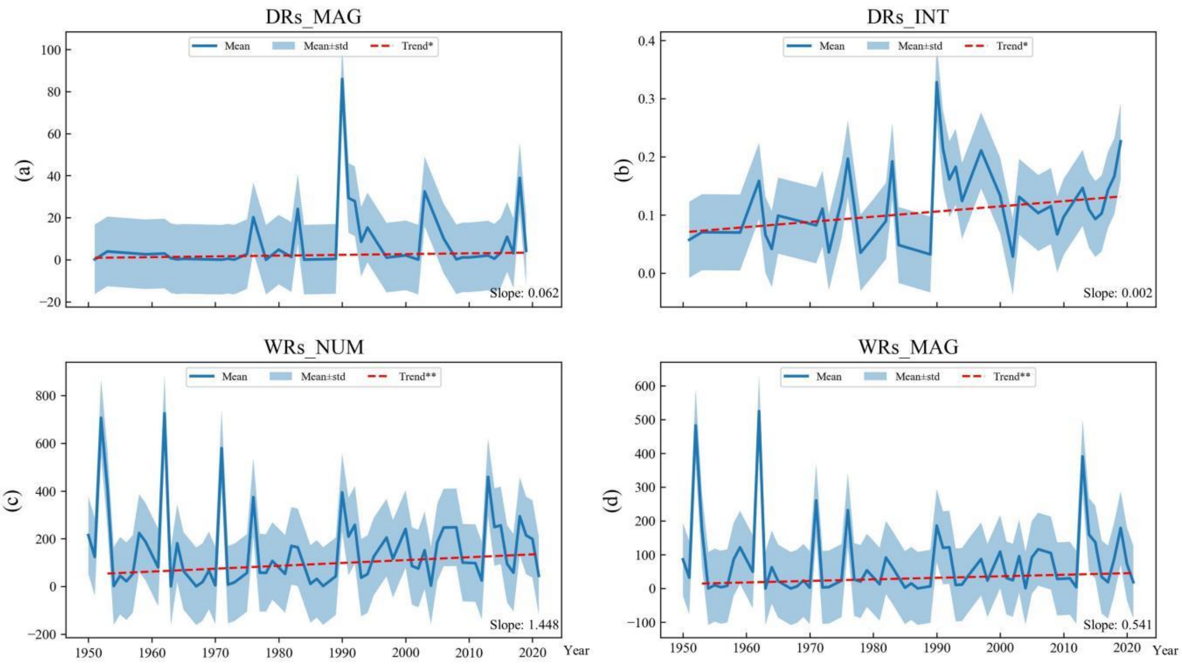

Figure 6. Long-term trends of compounding wet and dry extremes (CWDEs). Figures (a) and (b) depict the trends of CWDEs in magnitude (MAG) and intensity (INT) in dry regions (DRs) spanning the whole period. Figures (c) and (d) show the trends of CWDEs in NUM (number) and MAG in wet regions (WRs) from 1953

to 2021. All trends are determined by the M-K test, and the corresponding Sen's slopes are labeled at the right corner in each sub-figure. The value of the slope with one/two asterisk(s) indicate(s) that the trend passes the significant test $p \leq 0.1/p \leq 0.05$.

Table 2 Trends of compounding wet and dry extremes (CWDEs) in wet and dry regions

Regions	Variable	Period	Trend	Slope	Tau
DRs	NUM	1950-1973	Increasing*	3	0.281
		1978-1988	Increasing**	4	0.5411
	MAG	1950-2021	Increasing*	0.062	0.201
	INT	1950-2021	Increasing**	0.002	0.212
WRs	NUM	1953-2021	Increasing*	1.448	0.184
	MAG	1953-2021	Increasing**	0.541	0.181
	INT	1962-1974	Increasing**	0.024	0.455
		1973-1984	Decreasing**	0.383	0.491

Note: the variables NUM, MAG, and INT indicate the number, magnitude, and intensity of CWDEs. One and two asterisks (*) indicate that the trend passes the significant test $p \leq 0.1$ and $p \leq 0.05$, respectively.

4.3.3 Spatial clusters

Figures 7 (a) and (b) illustrate the raw distribution and clustering results of CSI. CWDEs exhibit a highly clustered pattern both in WRs and DRs, indicated by a GMI of 0.86. Additionally, the z score of the result (159) confirms that the clustered spatial pattern is not random with more than a 99% confidence level. The spatial distribution of CWDEs is delineated into five groups, from the highest to the lowest percentage, LL, NS, HH, HL, and LH take up 45%, 35%, 19%, 1%, and nearly zero (only three grid pixels) of WRs and DRs, respectively. Specifically, the LL cluster suggests the regions are less susceptible to CHMEs. Almost all regions labeled as LL are located in DRs and cover all northeastern parts of Germany, including most of the Elbe, Oder, and Warnow basins. The H-L cluster is distributed sparsely in northeastern Germany, these areas are slightly vulnerable to CWDEs. Normally, such a category implies a few regions affected by severe CWDEs distribute among massive neighborhoods which are insensitive to CWDEs.

More attention should be paid to two risky groups, including HH and LH clusters, as these groups are highly sensitive to CWDEs. The group of HH shows an intensive collection. Major regions (87%) are from WRs and are located in the southern tip of Germany. The rest of the regions mainly lie in the central parts of the

Elbe basin and a few areas (1%) are found in the northeastern Rhine basin. On the other hand, there are three LH grid cells found in the northwestern part of the Rhine basin. These are in the margin of the HH block and are exposed to a hidden danger when CWDEs occur on a large scale. Last but not least, some uncertainties exist about the NS group, there is still no obvious evidence to determine whether they will be impacted by CWDEs.

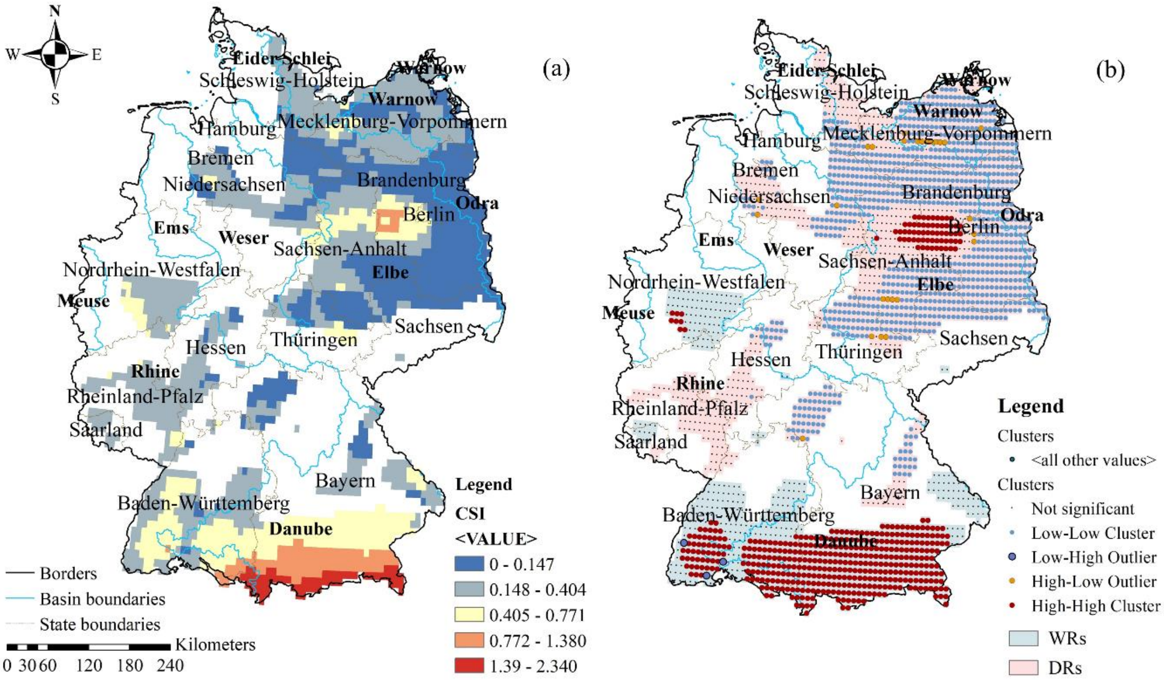

Figure 7. Risky pattern of compounding wet and dry extremes (CWDEs) across wet regions (WRs) and dry regions (DRs), Figure (a) is the original distribution, while Figure (b) shows the clustering result of CWDEs. Five clusters are identified and labeled with different colors and point sizes shown by the legend.

5 Discussions

5.1 The identification of CHMEs

Identifying CHMEs has been a challenge. Unlike individual extremes, the detection of the compound of multiple hazards not only involves overlapping features but also distinguishing threats from every constituent. The improved approach uses an independent identification method and scale to detect CWDEs within a limited window, which may yield more reliable results of CWDEs by considering individual components from evolving-based and impact-oriented perspectives. Compared to the copula theories (Sadegh et al. 2017) and complex networks (Boers et al. 2019), the study proposes an explicit definition and effective framework to identify CWDEs from analyzing concurrent events perspective. The method offers good flexibility and generalization since it avoids massive data to make fitting and/or intense computation and deep system knowledge (Raymond et al. 2020).

Moreover, our study stresses that a separate system is needed concerning distinct components of CWDEs. The indiscriminate use of a unified method extracting various hazards may deliver inaccurate information about compound extremes, one reason for this is the same identification window used for all hazards, which could ignore the different time effects of particular types of extremes. Additionally, SIM assumes a known distribution to find well-fitted parameters for most normal samples in the population (Laimighofer and Laaha 2022), inevitably abandoning the information of outliers from datasets. The loss of information may exclude extremely high and low values and further lead to greater uncertainties regarding CWDEs' identification. It is argued that the drawback of SIM caused by the generalizing process could be weakened when using a long accumulative process for detecting durable events. Still, the procedure can not be effective in exploring rapidly developing events, such as EWs. Hence, our study suggests a cautious application of SIM especially when adopting unified windows for detecting compound events involving short-lasting but devastating extremes.

5.2 The behaviors of CWDEs

On a monthly scale, the co-existence of EDs and EWs indicates the short and severe flash droughts before or after days with heavy rainfall. Such a drastic and fast transition between contrasting events within a single month could pose a great challenge to the resilience of ecosystems (Zhang et al. 2023, Bi et al. 2023, Shi et al. 2022). In addition, the summer season is characterized as the most vulnerable period to CWDEs. The severity of CWDEs could be exacerbated by summer heat waves (HWs) which have been observed with an increasing frequency and a spatial evolution from the northern to southern parts of Germany (Matzarakis et al. 2020). The combinations of HWs and CWDEs could give rise to high-impact wet-hot, dry-hot events, or both types, leading to massive devastation to urban infrastructure and ecological community (Gu et al. 2022, Obladen et al. 2021, Zscheischler et al. 2020). Even worse, the substantial uptrends in the magnitude and intensity of CWDEs have been determined both in DRs and WRs of Germany. It indicates that the occurrence of severer events could continuously increase under the changing climate, alarming the need for more attention and preparation to cope with the potential threats.

Furthermore, Morans' clustering analysis reveals the location and density of different groups that represent the five risk levels prone to CWDEs. It is observed that most of the events (80%) and hazardous areas (87%) related to CWDEs are concentrated in WRs in low-altitude regions. This finding suggests that a chronic moist environment could be conducive to severer CWDEs compared to a drier climate. Besides, a clear negative correlation is discovered between the performance of CWDEs and their geographical position, shown by the -0.6 Pearson coefficient (PC) and the -0.5 Spearman coefficient (SC). The fiercer CWDEs tend to strike mountainous terrain, where higher elevation exerts a great influence on local air temperature dynamics and further impacts convective movement (Arnoux et al. 2021). These variations directly contribute to complicated and volatile hydrometeorological processes and the occurrence of associated compounding anomalies. In light of the direct exposure to CWDEs, it is crucial to emphasize vegetation impact, as plants are expected to be more fragile during the period of CWDEs, such as several forests in the southern Rhine-Main and Danube Basin (Florian Süßel and Brüggemann 2021). In the Alps area, a region known as highly sensitive to climate change (Arnoux et al. 2021), the CWDEs may disturb the ecological stability of grasslands and water balance.

5.3 The attributions of CWDEs

As a bivariate hazard, changes in CWDEs are attributed to variations in EDs and EWs. Therefore, we further conduct a correlation analysis between EDs/EWs and CWDEs, the results are shown in Figure B.2 in the Supplementary and Appendix Data. The severity of CHMEs in WRs is more associated with EDs (0.84 in PC and 0.87 SC) than EWs (0.56 in PC and 0.46 SC), which indicates that variations of EDs are more influential in developing visible changes in CWDEs. It is generally verified by a homogeneous distribution of EWs with a comparable level but a heterogeneous pattern of EDs among all CWDEs in WRs, as shown in Figures B.3 (a) and (c) in the Supplementary and Appendix Data. Based on the dominance of EDs to CWDEs, the southeast regions in the Danube basin in WRs are stressed additionally. These areas could encounter high-impact EDs and CWDEs in the future as the decreasing number but the increasing magnitude of EDs has been examined (Figure 4 (d)-(e)).

In contrast, the emergence of CWDEs in DRs is more easily facilitated by EWs, as demonstrated by PC of 0.93 and SC of 0.81. Therefore, the study places extra emphasis on northern parts of Germany considering possible CWDEs caused by increasing EWs in (Figure 4 (a)-(c)). Particularly, a few regions located in the state of Brandenburg should raise major concerns due to the uptrend founded in *INT* of EWs. The more dispersed distribution of *INT* of EWs implies a more powerful control on CWDEs in DRs, shown by Figure B.3 (c) in the Supplementary and Appendix Data. It is reported that economic damage in the state of Brandenburg inflicted by EDs solely has reached around 72 million euros, and 77.54% of the total agricultural land fell within the high drought zones during the event in 2018 (Ihinegbu et al. 2022). Extra threats coming from the increasing occurrence of CWDEs could aggravate soil erosion and land degradation (Chen et al. 2020, Handwerger et al. 2019). Therefore, as a big crop-exporting country, the study calls attention to food security as the identified areas of CWDEs are mainly responsible for planting main crops (e.g., wheat, and potatoes).

5.4 Limitations and Outlook

There are still some limitations in the current work that require further exploration. First of all, uncertainties could exist in the input. Reanalysis data present potential errors compared with ground observations obtained from the Federal Institute of Hydrology (Figure B.4 in the Supplementary and Appendix Data). For example, they overestimate some low values in the northeastern part of Germany. However, the general distribution compares well to the observational data at point gauges (Rivoire et al. 2021, Gomis-Cebolla et al. 2023, Wu et al. 2023). As a result, they could effectively capture the climatic division and identify events.

Second, the study focuses on a single key driving force (precipitation) for characterizing CWDEs. The ignorance of other climatic and anthropogenic factors could compromise the accuracy of identified extremes (Brunner et al. 2022, Stuart-Smith et al. 2021). For example, snow and temperature are other crucial indices influencing the behaviors of HMEs referencing snow-melting floods and hot-dry events in Germany (Krug et al. 2020, Merz et al. 2020, Steidinger et al. 2022, Zscheischler and Fischer 2020). At the same time, the formation and impact of HMEs can be either alleviated or aggravated by human activities (Jehanzaib et al. 2020, Pirnia et al. 2019a, 2019b, Shao and Kam 2020, Zhang et al. 2022), typically reservoir regulation, agricultural irrigation, and land surface changes caused by urbanization processes. Therefore, a comprehensive system involving more crucial drivers could be a focal issue in detecting CWDEs in future studies.

Lastly, more future investigations should prioritize the examination of the successive changes within the inner dynamics of CWDEs and their teleconnections with climate variations. Previous studies have revealed that stable and robust teleconnections exist between climate variations and dry/wet oscillations on a large scale, particularly the strong influence of the North Atlantic Oscillation on short-term fluctuations of extreme events in Europe (De Luca et al. 2020, Sun et al. 2016). However, the linkage between climate change and CWDEs at a local scale remains unclear.

6 Conclusions

Due to climate change, more frequent and severe CHMEs are expected to occur in the future. To deepen the understanding of CHMEs, the study proposes a separate system to explore a new category of compounding hazards based on SIM and POT in two different time scales. Long-term spatiotemporal variations and risky patterns of CWDEs are fully investigated in Germany by using OLS, M-K test, GMI, and RMI respectively.

Our findings reveal a strong seasonal effect of CWDEs where the summer season undergoes the most serious events while winter is the most resilient period. Long-term robust increases in different aspects of CWDEs are observed both in DRs and WRs. Furthermore, the highly clustered pattern of the spatial distribution of CWDEs is determined, which indicates more hazardous areas are mainly located in the south of Baden-Württemberg State in the Rhine basin and Bavaria in the Danube basin, as well as in some parts next to Berlin. In addition, we uncover that chronic wet conditions and complex mountainous geography could induce severe CWDEs. Based on strong links between EWs (EDs) and CWDEs in DRs (WRs), we further highlight that several areas could frequently experience disastrous CWDEs in the future, including the state of Brandenburg and southeast regions in the Danube basin. Therefore, there is a pressing need for applicable approaches and management frameworks within these areas to enhance ecological resilience and effectively mitigate the impacts of CWDEs.

Moreover, the study calls for more attention to compounding HMEs with distinct features and highlights the different time effects of wet and dry events in the study. The proposed framework can also be applied to other regions due to explicit methods and open data sources and can be extended to other CHMEs by employing EWs with other types of drought phenomena (e.g., agricultural, soil moisture, and socio-economic droughts). For future studies, we appeal to the comprehensive identification of CWDEs by incorporating additional information on local hydrological and water management factors (e.g., catchment characteristics, groundwater level, reservoir operation, etc.). Last but not least, studies on driving forces and impacting mechanisms of CWDEs will greatly benefit hazard preparations and adaptation planning during the climate-changing process.

Acknowledgments

The first author gratefully acknowledges China Scholarship Council for the financial support (No. 202106380061). The work is supported by the Technical University of Munich under the framework of TUM Innovation Network "EarthCare" funded under the Excellence Strategy of the Federal Government and the Länder. The authors would like to thank the editors and anonymous reviewers for their time and insightful comments in reviewing this paper.

References

Abbate, A., Papini, M. Longoni, L., 2021. Analysis of meteorological parameters triggering rainfall-induced landslide: a review of 70 years in Valtellina. Natural Hazards and Earth System Sciences 21(7), 2041-2058.

Ahmed, K., Shahid, S., Wang, X., Nawaz, N., Khan, N., 2019. Spatiotemporal changes in aridity of Pakistan during 1901-2016. Hydrology and Earth System Sciences, 23(7), 3081-3096.

Agarwal, A., Yuan, N., Cheung, K.K. Shukla, R., 2022. Emerging Hydro-Climatic Patterns, Teleconnections, and Extreme Events in Changing World at Different Timescales, p. 56, Multidisciplinary Digital Publishing Institute.

Ali, M., Deo, R.C., Maraseni, T. Downs, N.J., 2019. Improving SPI-derived drought forecasts incorporating synoptic-scale climate indices in multi-phase multivariate empirical mode decomposition model hybridized with simulated annealing and kernel ridge regression algorithms. Journal of Hydrology 576, 164-184.

Allan, R.P., Soden, B.J., John, V.O., Ingram, W. Good, P., 2010. Current changes in tropical precipitation. Environmental Research Letters 5(2), 025205.

Anderson, T.G., Anchukaitis, K.J., Pons, D. Taylor, M., 2019. Multiscale trends and precipitation extremes in the Central American Midsummer Drought. Environmental Research Letters 14(12), 124016.

Apurv, T., Sivapalan, M. Cai, X.M., 2017. Understanding the Role of Climate Characteristics in Drought Propagation. Water Resources Research 53(11), 9304-9329.

Arnoux, M., Brunner, P., Schaefli, B., Mott, R., Cochand, F. Hunkeler, D., 2021. Low-flow behavior of alpine catchments with varying quaternary cover under current and future climatic conditions. Journal of Hydrology 592.

Bachmair, S., Svensson, C., Hannaford, J., Barker, L., Stahl, K., 2016. A quantitative analysis to objectively appraise drought indicators and model drought impacts. Hydrology and Earth System Sciences 20(7), 2589-2609.

Becker, A. Grünewald, U., 2003. Flood risk in central Europe. Science Policy Forum 300(5622), p. 1099.

Bermudez, M., Farfan, J.F., Willems, P. Cea, L., 2021. Assessing the Effects of Climate Change on Compound Flooding in Coastal River Areas. Water Resources Research 57(10), e2020WR029321.

Bi, W., Weng, B., Yan, D., Wang, M., Wang, H., Jing, L. Yan, S., 2022. Soil phosphorus loss increases under drought-flood abrupt alternation in summer maize planting area. Agricultural Water Management, 262, p.107426.

Bi, W., Li, M., Weng, B., Yan, D., Dong, Z., Feng, J., Wang, H., 2023. Drought-flood abrupt alteration events over China. Science of The Total Environment, 875, 162529.

BKG - Bundesamt für Kartographie und Geodäsie, 2015. Geographische Namen 1: 250.000. GeoBasis-DE. (Geographical names 1:250,000).

BKG - Bundesamt für Kartographie und Geodäsie, 2017. Geographische Namen 1: 250.000. GeoBasis-DE. (Geographical names 1:250,000).

Blöschl, G., Nester, T., Komma, J., Parajka, J., Perdigão, R.A.P., 2013. The June 2013 flood in the Upper Danube Basin, and comparisons with the 2002, 1954 and 1899 floods. Hydrology and Earth System Sciences 17(12), 5197-5212.

Blöschl, G., Szolgay, J., Parajka, J., Kohnova, S. Miklanek, P., 2016. Thematic issue on floods in the Danube basin-processes, patterns, predictions. Journal of Hydrology Hydromechanics 64(4), 301.

Boers, N., Goswami, B., Rheinwalt, A., Bookhagen, B., Hoskins, B. Kurths, J., 2019. Complex networks reveal global pattern of extreme-rainfall teleconnections. Nature 566(7744), 373-377.

Brunner, M.I., Swain, D.L., Wood, R.R., Willkofer, F., Done, J.M., Gilleland, E. Ludwig, R., 2021. An extremeness threshold determines the regional response of floods to changes in rainfall extremes. Communications Earth & Environment 2(1), article id. 173..

Brunner, M.I., Van Loon, A.F. Stahl, K., 2022. Moderate and severe hydrological droughts in Europe differ in their hydrometeorological drivers. Water Resources Research 58(10), e2022WR032871.

Center, N.D.M., 2018. North American Drought Monitor. https://droughtmonitor.unl.edu/, University of Nebraska-Lincoln, U.S.A. Accessed 21 April 2023.

Chen, H., Wang, S. Wang, Y., 2020. Exploring Abrupt Alternations Between Wet and Dry Conditions on the Basis of Historical Observations and Convection-Permitting Climate Model Simulations. Journal of Geophysical Research-Atmospheres 125(9), e2019JD031982.

Chowdhuri, I., Pal, S.C., Saha, A., Chakrabortty, R., Roy, P., 2022. Mapping of earthquake hotspot and coldspot zones for identifying potential landslide hotspot areas in the Himalayan region. Bulletin of Engineering Geology and the Environment 81(7), 257.

Ciccarese, G., Mulas, M., Alberoni, P.P., Truffelli, G. Corsini, A., 2020. Debris flows rainfall thresholds in the Apennines of Emilia-Romagna (Italy) derived by the analysis of recent severe rainstorms events and regional meteorological data. Geomorphology 358, 107097.

CSIRO, 2014. State of the Climate 2014, CSIRO.

De Luca, P., Messori, G., Wilby, R.L., Mazzoleni, M. Di Baldassarre, G., 2020. Concurrent wet and dry hydrological extremes at the global scale. Earth System Dynamics 11(1), 251-266.

Donat, M.G., Lowry, A.L., Alexander, L.V., O'Gorman, P.A. Maher, N., 2016. More extreme precipitation in the world's dry and wet regions. Nature Climate Change 6(5), 508-513.

EEA - European Environment Agency, 2016. European Digital Elevation Model (EUDEM), version 1.1.

Erfurt, M., Glaser, R. Blauhut, V., 2019. Changing impacts and societal responses to drought in southwestern Germany since 1800. Regional Environmental Change 19(8), 2311-2323.

Feng, S.F., Hao, Z.C., Wu, X.Y., Zhang, X. Hao, F.H., 2021. A multi-index evaluation of changes in compound dry and hot events of global maize areas. Journal of Hydrology 602, 126728.Franzke, C.L. (2021) Towards the development of economic damage functions for weather and climate extremes. Ecological Economics 189, 107172.

Garg, S. Mishra, V., 2019. Role of Extreme Precipitation and Initial Hydrologic Conditions on Floods in Godavari River Basin, India. Water Resources Research 55(11), 9191-9210.

Gocic, M. Trajkovic, S., 2013. Analysis of changes in meteorological variables using Mann-Kendall and Sen's slope estimator statistical tests in Serbia. Global and Planetary Change 100, 172-182.

Gomis-Cebolla, J., Rattayova, V., Salazar-Galán, S., Francés, F., 2023. Evaluation of ERA5 and ERA5-Land reanalysis precipitation datasets over Spain (1951–2020). Atmospheric Research, 284, 106606.

Gu, L., Chen, J., Yin, J., Slater, L.J., Wang, H.M., Guo, Q., Feng, M., Qin, H. Zhao, T., 2022. Global Increases in Compound Flood-Hot Extreme Hazards Under Climate Warming. Geophysical Research Letters 49(8).

Han, J., Du, H., Wu, Z., He, H. S., 2019. Changes in extreme precipitation over dry and wet regions of China during 1961-2014. Journal of Geophysical Research: Atmospheres, 124(11), 5847-5859.

Handwerger, A.L., Huang, M. H., Fielding, E.J., Booth, A.M. Bürgmann, R., 2019. A shift from drought to extreme rainfall drives a stable landslide to catastrophic failure. Scientific Reports 9(1), 1-12.

Hellwig, J., de Graaf, I., Weiler, M. Stahl, K., 2020. Large-scale assessment of delayed groundwater responses to drought. Water Resources Research 56(2), e2019WR025441.

Hu, G. Franzke, C.L., 2020. Evaluation of daily precipitation extremes in reanalysis and gridded observation-based data sets over Germany. Geophysical Research Letters 47(18), e2020GL089624.

Huang, J., Hu, T., Yasir, M., Gao, Y., Chen, C., Zhu, R., Wang, X., Yuan, H., Yang, J., 2019. Root growth dynamics and yield responses of rice (Oryza sativa L.) under drought—Flood abrupt alternating conditions. Environmental and Experimental Botany, 157, pp.11-25.

Ihinegbu, C., Ogunwumi, T., 2022. Multi-criteria modelling of drought: a study of Brandenburg Federal State, Germany. Modeling Earth Systems and Environment, 8(2), pp.2035-2049.

Iizumi, T., Ramankutty, N., 2015. How do weather and climate influence cropping area and intensity? Global food security 4, 46-50.

Jang, J.H., Chang, T.H., 2022. Flood risk estimation under the compound influence of rainfall and tide. Journal of Hydrology 606, 127446.

Jehanzaib, M., Shah, S.A., Yoo, J., Kim, T.W., 2020. Investigating the impacts of climate change and human activities on hydrological drought using non-stationary approaches. Journal of Hydrology 588, 125052.

Ji, Z., Li, N., Wu, X., 2017. Threshold determination and hazard evaluation of the disaster about drought/flood sudden alternation in Huaihe River basin, China. Theoretical and Applied Climatology 133(3-4), 1279-1289.

Kaiser, M., Günnemann, S., Disse, M., 2021. Spatiotemporal analysis of heavy rain-induced flood occurrences in Germany using a novel event database approach. Journal of Hydrology 595, 125985.

Kalisa, W., Igbawua, T., Ujoh, F., Aondoakaa, I. S., Namugize, J. N., Zhang, J., 2021. Spatio-temporal variability of dry and wet conditions over East Africa from 1982 to 2015 using quantile regression model. Natural Hazards, 106, 2047-2076. https://doi.org/10.1007/s11069-021-04530-1.

Kendall, M.G., 1948. Rank correlation methods. Charles Griffin, London.

Klöckner, J., 2020. Understanding Farming-Facts and figures about German farming. Federal Ministry of Food and Agriculture.

Kreibich, H., Van Loon, A.F., Schröter, K., Ward, P.J., Mazzoleni, M., Sairam, N., Abeshu, G.W., Agafonova, S., AghaKouchak, A., Aksoy, H., 2022. The challenge of unprecedented floods and droughts in risk management. Nature 608(7921), 80-86.

Krug, A., Primo, C., Fischer, S., Schumann, A., Ahrens, B., 2020. On the temporal variability of widespread rain-on-snow floods. Meteorologische Zeitschrift 29(2), 147-163.

Lai, Y.C., Li, J.F., Gu, X.H., Liu, C.C., Chen, Y.D., 2021. Global Compound Floods from Precipitation and Storm Surge: Hazards and the Roles of Cyclones. Journal of Climate 34(20), 8319-8339.

Laimighofer, J., Laaha, G., 2022. How standard are standardized drought indices? Uncertainty components for the SPI & SPEI case. Journal of Hydrology 613, 128385.

Leonard, M., Westra, S., Phatak, A., Lambert, M., van den Hurk, B., McInnes, K., Risbey, J., Schuster, S., Jakob, D., Stafford-Smith, M., 2013. A compound event framework for understanding extreme impacts. WIREs Climate Change 5(1), 113-128.

LfU, Bavaria's water authorities 2017 Augsburg.

Li, G., Yu, Z., Li, Y., Li, Z., Ju, Q., Huang, Y., 2023. The evolution of precipitation and its physical mechanisms in arid and humid regions of the Tibetan Plateau. Atmospheric Research, 285, 106638.

Lin, K., Chen, H., Xu, C.-Y., Yan, P., Lan, T., Liu, Z., Dong, C.J., 2020. Assessment of flash flood risk based on improved analytic hierarchy process method and integrated maximum likelihood clustering algorithm. Journal of Hydrology 584, 124696.

Liu, C., Zhang, X., Wang, T., Chen, G., Zhu, K., Wang, Q., Wang, J., 2022. Detection of vegetation coverage changes in the Yellow River Basin from 2003 to 2020. Ecological Indicators 138, 108818.

Liu, J., Jia, J., Yang, Y., Tang, M., Xue, Y., Lu, H., 2018. December. Risk Assessment for Drought-flood Abrupt Alternation in the Pearl River Basin, China. In IOP Conference Series: Materials Science and Engineering (Vol. 452, No. 2, p. 022029). IOP Publishing.

Lucas, R.A., Epstein, Y., Kjellstrom, T., 2014. Excessive occupational heat exposure: a significant ergonomic challenge and health risk for current and future workers. Extreme physiology & medicine 3, 1-8.

Mann, H.B., 1945. Nonparametric tests against trend. Econometrica 13, 245-259.

Matanó, A., de Ruiter, M.C., Koehler, J., Ward, P.J., Van Loon, A.F., 2022. Caught Between Extremes: Understanding Human-Water Interactions During Drought-To-Flood Events in the Horn of Africa. Earth's Future 10(9), e2022EF002747.

Matzarakis, A., Laschewski, G., Muthers, S., 2020. The Heat Health Warning System in Germany—Application and Warnings for 2005 to 2019. Atmosphere 11(2), 170.

McKee, T.B., Doesken, N.J., Kleist, J., 1993. The relationship of drought frequency and duration to time scales, pp. 179-183, Boston, MA, USA.

Merz, B., Dung, N.V., Apel, H., Gerlitz, L., Schröter, K., Steirou, E., Vorogushyn, S., 2018. Spatial coherence of flood-rich and flood-poor periods across Germany. Journal of Hydrology 559, 813-826.

Merz, R., Tarasova, L., Basso, S., 2020. The flood cooking book: ingredients and regional flavors of floods across Germany. Environmental Research Letters 15(11), 114024.

Meyer, J., Neuper, M., Mathias, L., Zehe, E., Pfister, L., 2020. More frequent flash flood events and extreme precipitation favouring atmospheric conditions in temperate regions of Europe. Hydrology and Earth System Sciences 26, 6163-6183.

Mukherjee, S., Mishra, A.K., 2021. Increase in Compound Drought and Heatwaves in a Warming World. Geophysical Research Letters 48(1), e2020GL090617.

News, 2019. From Drought to Flooding Rains as Farmers Celebrate Drenching in Queensland's West, ABC News. https://www.abc.net.au/news/rural/2019-02-04/from-drought-to-flooding-rains-in-western-queensland/10776576, accessed 21 April, 2023

Nyeko-Ogiramoi, P., Willems, P., Ngirane-Katashaya, G., 2013. Trend and variability in observed hydrometeorological extremes in the Lake Victoria basin. Journal of Hydrology 489, 56-73.

Obladen, N., Dechering, P., Skiadaresis, G., Tegel, W., Keßler, J., Höllerl, S., Kaps, S., Hertel, M., Dulamsuren, C., Seifert, T., Hirsch, M., 2021. Tree mortality of European beech and Norway spruce induced by 2018-2019 hot droughts in central Germany. Agricultural and Forest Meteorology, 307(2021), p.108482.

Pal, I., Al-Tabbaa, A., 2011. Assessing seasonal precipitation trends in India using parametric and non-parametric statistical techniques. Theoretical and applied climatology 103, 1-11.

Parry, S., Marsh, T., Kendon, M., 2013. 2012: From drought to floods in England and Wales. Weather 68(10), 268-274.

Parajka, J., Perdigão, R.A., 2013. The June 2013 flood in the Upper Danube Basin, and comparisons with the 2002, 1954 and 1899 floods. J Hydrology Earth System Sciences 17(12), 5197-5212.

Pirnia, A., Darabi, H., Choubin, B., Omidvar, E., Onyutha, C., Haghighi, A.T., 2019a. Contribution of climatic variability and human activities to stream flow changes in the Haraz River basin, northern Iran. Journal of Hydro-Environment Research 25, 12-24.

Pirnia, A., Golshan, M., Darabi, H., Adamowski, J., Rozbeh, S., 2019b. Using the Manna-Kendall test and double mass curve method to explore stream flow changes in response to climate and human activities. Journal of Water Climate Change 10(4), 725-742.

Poschlod, B., Zscheischler, J., Sillmann, J., Wood, R. R., Ludwig, R., 2020. Climate change effects on hydrometeorological compound events over southern Norway. Weather and climate extremes, 28, 100253.

Pour, S. H., Abd Wahab, A. K., Shahid, S., 2020. Spatiotemporal changes in aridity and the shift of drylands in Iran. Atmospheric Research, 233, 104704.

Qiang, Y., 2019. Flood exposure of critical infrastructures in the United States. International Journal of Disaster Risk Reduction 39, 101240.

Qiao, Y., Xu, W., Meng, C., Liao, X., Qin, L., 2022. Increasingly dry/wet abrupt alternation events in a warmer world: Observed evidence from China during 1980–2019. International Journal of Climatology 42(12), 6429-6440.

Raymond, C., Horton, R.M., Zscheischler, J., Martius, O., AghaKouchak, A., Balch, J., Bowen, S.G., Camargo, S.J., Hess, J., Kornhuber, K., Oppenheimer, M., Ruane, A.C., Wahl, T., White, K., 2020. Understanding and managing connected extreme events. Nature Climate Change 10(7), 611-621.

Report, 2022. Drought in Europe August 2022. GDO Analytical Report, EU.

Ridder, N.N., Ukkola, A.M., Pitman, A.J., Perkins-Kirkpatrick, S.E., Science, A., 2022. Increased occurrence of high impact compound events under climate change. Climate and Atmospheric Science 5(1), 1-8.

Ridder, N.N., Pitman, A.J., Westra, S., Ukkola, A., Do, H.X., Bador, M., Hirsch, A.L., Evans, J.P., Di Luca, A., Zscheischler, J., 2020. Global hotspots for the occurrence of compound events. Nature Communications 11(1), 1-10.

Rivoire, P., Martius, O., Naveau, P.J.E., Science, S., 2021. A comparison of moderate and extreme ERA-5 daily precipitation with two observational data sets. Earth and Space Science 8(4), e2020EA001633.

Sadegh, M., Moftakhari, H., Gupta, H.V., Ragno, E., Mazdiyasni, O., Sanders, B., Matthew, R., AghaKouchak, A., 2018. Multihazard Scenarios for Analysis of Compound Extreme Events. Geophysical Research Letters 45(11), 5470-5480.

Sadegh, M., Ragno, E., AghaKouchak, A., 2017. Multivariate Copula A nalysis T oolbox (MvCAT): describing dependence and underlying uncertainty using a Bayesian framework. Water Resources Research 53(6), 5166-5183.

Saharia, A.M., Zhu, Z.D., Atkinson, J.F., 2021. Compound flooding from lake seiche and river flow in a freshwater coastal river. Journal of Hydrology 603, 126969.

Salvador, C., Nieto, R., Linares, C., Diaz, J., Gimeno, L., 2020. Short-term effects of drought on daily mortality in Spain from 2000 to 2009. Environmental Research 183, 109200.

Scharnweber, T., Manthey, M., Criegee, C., Bauwe, A., Schröder, C., Wilmking, M., 2011. Drought matters–Declining precipitation influences growth of Fagus sylvatica L. and Quercus robur L. in north-eastern Germany. Forest Ecology and Management, 262(6), 947-961.

Schuldt, B., Buras, A., Arend, M., Vitasse, Y., Beierkuhnlein, C., Damm, A., Gharun, M., Grams, T.E., Hauck, M., Hajek, P.J.B., Ecology, A., 2020. A first assessment of the impact of the extreme 2018 summer drought on Central European forests. Basic and applied Ecology 45, 86-103.

Schumacher, D.L., Keune, J., Van Heerwaarden, C.C., Vilà-Guerau de Arellano, J., Teuling, A.J., Miralles, D.G., 2019. Amplification of mega-heatwaves through heat torrents fuelled by upwind drought. Nature Geoscience 12(9), 712-717.

Schurer, A. P., Ballinger, A. P., Friedman, A. R., Hegerl, G. C., 2020. Human influence strengthens the contrast between tropical wet and dry regions. Environmental Research Letters, 15(10), 104026.

Sen, P.K., 1968. Estimates of the regression coefficient based on Kendall's tau. Journal of the American statistical association 63(324), 1379-1389.

Shan, L., Zhang, L., Song, J., Zhang, Y., She, D., Xia, J., 2018. Characteristics of dry-wet abrupt alternation events in the middle and lower reaches of the Yangtze River Basin and the relationship with ENSO. Journal of Geographical Sciences 28(8), 1039-1058.

Shao, W., Kam, J., 2020. Retrospective and prospective evaluations of drought and flood. J Science of The Total Environment 748, 141155.

Shi, W., Huang, S., Liu, D., Huang, Q., Leng, G., Wang, H., Fang, W., Han, Z., 2020. Dry and wet combination dynamics and their possible driving forces in a changing environment. Journal of Hydrology 589, 125211.

Steidinger, B.S., Büntgen, U., Stobbe, U., Tegel, W., Sproll, L., Haeni, M., Moser, B., Bagi, I., Bonet, J.A., Buée, M., Dauphin, B., 2022. The fall of the summer truffle: Recurring hot, dry summers result in declining fruitbody production of Tuber aestivum in Central Europe. Global Change Biology, 28(24), pp.7376-7390.

Stuart-Smith, R., Roe, G., Li, S., Allen, M., 2021. Increased outburst flood hazard from Lake Palcacocha due to human-induced glacier retreat. Nature Geoscience 14(2), 85-90.

Sun, Q., Miao, C., AghaKouchak, A., Duan, Q., 2016. Century-scale causal relationships between global dry/wet conditions and the state of the Pacific and Atlantic Oceans. Geophysical Research Letters 43(12), 6528-6537.

Süßel, F., Brüggemann, W., 2021. Tree water relations of mature oaks in southwest Germany under extreme drought stress in summer 2018. Plant Stress, 1, 100010.

Tabari, H., Hosseinzadehtalaei, P., Thiery, W., Willems, P., 2021. Amplified drought and flood risk under future socioeconomic and climatic change. Earth's Future 9(10), e2021EF002295.

Tan, X., Wu, X., Huang, Z., Fu, J., Tan, X., Deng, S., Liu Y., Gan TY., Liu, B., 2023. Increasing global precipitation whiplash due to anthropogenic greenhouse gas emissions. Nature Communications, 14(1), 2796

Thomas, J., Prasannakumar, V., 2016. Temporal analysis of rainfall (1871–2012) and drought characteristics over a tropical monsoon-dominated State (Kerala) of India. Journal of Hydrology 534, 266-280.

Tian, R., Cao, C., Peng, L., Ma, G., Bao, D., Guo, J., Yomwan, P., 2014. The use of HJ-1A/B satellite data to detect changes in the size of wetlands in response in to a sudden turn from drought to flood in the middle and lower reaches of the Yangtze River system in China. Geomatics, Natural Hazards and Risk 7(1), 287-307.

Treppiedi, D., Cipolla, G., Francipane, A., Noto, L.J., 2021. Detecting precipitation trend using a multiscale approach based on quantile regression over a Mediterranean area. International Journal of Climatology 41(13), 5938-5955.

Tyagi, S., Zhang, X., Saraswat, D., Sahany, S., Mishra, S.K., Niyogi, D., 2022. Flash Drought: Review of Concept, Prediction and the Potential for Machine Learning, Deep Learning Methods. Earth's Future 10(11), e2022EF002723.

Ullah, S., You, Q., Sachindra, D., Nowosad, M., Ullah, W., Bhatti, A. S., Jin, Z., Ali, A., 2022. Spatiotemporal changes in global aridity in terms of multiple aridity indices: An assessment based on the CRU data. Atmospheric Research, 268, 105998. https://doi.org/10.1016/j.atmosres.2021.105998

Visser-Quinn, A., Beevers, L., Collet, L., Formetta, G., Smith, K., Wanders, N., Thober, S., Pan, M. and Kumar, R., 2019. Spatio-temporal analysis of compound hydro-hazard extremes across the UK. Advances in Water Resources 130, 77-90.

Vogel, J., Paton, E., Aich, V., Bronstert, A., 2021. Increasing compound warm spells and droughts in the Mediterranean Basin. Weather and Climate Extremes 32, 100312.

Wang, F., Shao, W., Yu, H.J., Kan, G.Y., He, X.Y., Zhang, D.W., Ren, M.L., Wang, G., 2020. Re-evaluation of the Power of the Mann-Kendall Test for Detecting Monotonic Trends in Hydrometeorological Time Series. Frontiers in Earth Science 8.

Wieland, M., Martinis, S., 2020. Large-scale surface water change observed by Sentinel-2 during the 2018 drought in Germany. International Journal of Remote Sensing 41(12), 4742-4756.

Wilhite, D.A., 2006. Drought monitoring and early warning: Concepts, progress and future challenges. WMO - No. 1006. Geneva, Switzerland.

Wu, J.F., Yao, H.X., Chen, X.H., Wang, G.X., Bai, X.Y., Zhang, D.J., 2022. A framework for assessing compound drought events from a drought propagation perspective. Journal of Hydrology 604, 127228.

Wu, X., Su, J., Ren, W., Lü, H., Yuan, F., 2023. Statistical comparison and hydrological utility evaluation of ERA5-Land and IMERG precipitation products on the Tibetan Plateau. Journal of Hydrology, 620, p.129384.

Xu, H., Chen, H., Wang, H., 2022. Future changes in precipitation extremes across China based on CMIP6 models. International Journal of Climatology, 42(1), pp.635-651.

Yang, Y., Zhao, N., Wang, Y., Chen, M., 2022. Variations in summertime compound heat extremes and their connections to urbanization in China during 1980–2020. Environmental Research Letters 17(6), 064024.

Zhang, T., Su, X., Zhang, G., Wu, H., Wang, G., Chu, J., 2022. Evaluation of the impacts of human activities on propagation from meteorological drought to hydrological drought in the Weihe River Basin, China. Science of Total Environment 819, 153030.

Zhang, W., Luo, M., Gao, S., Chen, W., Hari, V., Khouakhi, A., 2021. Compound Hydrometeorological Extremes: Drivers, Mechanisms and Methods. Frontiers in Earth Science 9.

Zhang, Y., You, Q., Ullah, S., Chen, C., Shen, L., Liu, Z., 2023. Substantial increase in abrupt shifts between drought and flood events in China based on observations and model simulations. Science of The Total Environment, 876, p.162822.

Zscheischler, J., Fischer, E.M., 2020. The record-breaking compound hot and dry 2018 growing season in Germany. Weather and Climate Extremes 29, 100270.

Zscheischler, J., Fischer, E.M., Lange, S., 2019. The effect of univariate bias adjustment on multivariate hazard estimates. Earth System Dynamics 10(1), 31-43.

Zscheischler, J., Seneviratne, S.I., 2017. Dependence of drivers affects risks associated with compound events. Sci. Adv. 3 https://doi.org/10.1126/sciadv.1700263.

Zscheischler, J., Westra, S., van den Hurk, B.J.J.M., Seneviratne, S.I., Ward, P.J., Pitman, A., AghaKouchak, A., Bresch, D.N., Leonard, M., Wahl, T. and Zhang, X., 2018. Future climate risk from compound events. Nature Climate Change 8(6), 469-477.

Zuzani, P., Ngongondo, C., Mwale, F., Willems, P., 2019. Examining trends of hydro-meteorological extremes in the Shire River Basin in Malawi. Physics and Chemistry of the Earth, Parts A/B/C 112, 91-102.